

## **Intrinsic fluorescence for cervical precancer detection using polarized light based in-house fabricated portable device**

Bharat Lal Meena  
Pankaj Singh  
Amar Nath Sah  
Kiran Pandey  
Asha Agarwal  
Chayanika Pantola  
Asima Pradhan

# Intrinsic fluorescence for cervical precancer detection using polarized light based in-house fabricated portable device

Bharat Lal Meena,<sup>a,b</sup> Pankaj Singh,<sup>a,c</sup> Amar Nath Sah,<sup>d</sup> Kiran Pandey,<sup>e</sup> Asha Agarwal,<sup>f</sup> Chayanika Pantola,<sup>g</sup> and Asima Pradhan<sup>a,h,\*</sup>

<sup>a</sup>Indian Institute of Technology Kanpur, Department of Physics, Kanpur, Uttar Pradesh, India

<sup>b</sup>University of Rajasthan, Department of Physics, Jaipur, Rajasthan, India

<sup>c</sup>LSM Government PG College, Department of Physics, Pithoragarh, Uttarakhand, India

<sup>d</sup>Indian Institute of Technology Kanpur, Department of Biological Sciences and Bioengineering, Kanpur, Uttar Pradesh, India

<sup>e</sup>GSVM Medical College, Department of Obstetrics and Gynaecology, Kanpur, Uttar Pradesh, India

<sup>f</sup>Regency Hospital, Department of Pathology, Kanpur, Uttar Pradesh, India

<sup>g</sup>LPS Institute of Cardiology, Department of Pathology, Kanpur, Uttar Pradesh, India

<sup>h</sup>Indian Institute of Technology Kanpur, Center for Lasers and Photonics, Kanpur, Uttar Pradesh, India

**Abstract.** An in-house fabricated portable device has been tested to detect cervical precancer through the intrinsic fluorescence from human cervix of the whole uterus in a clinical setting. A previously validated technique based on simultaneously acquired polarized fluorescence and polarized elastic scattering spectra from a turbid medium is used to extract the intrinsic fluorescence. Using a diode laser at 405 nm, intrinsic fluorescence of flavin adenine dinucleotide, which is the dominant fluorophore and other contributing fluorophores in the epithelium of cervical tissue, has been extracted. Different grades of cervical precancer (cervical intraepithelial neoplasia; CIN) have been discriminated using principal component analysis-based Mahalanobis distance and linear discriminant analysis. Normal, CIN I and CIN II samples have been discriminated from one another with high sensitivity and specificity at 95% confidence level. This *ex vivo* study with cervix of whole uterus samples immediately after hysterectomy in a clinical environment indicates that the in-house fabricated portable device has the potential to be used as a screening tool for *in vivo* precancer detection using intrinsic fluorescence. © 2018 Society of Photo-Optical Instrumentation Engineers (SPIE) [DOI: 10.1117/1.JBO.23.1.015005]

Keywords: cervical cancer; intrinsic fluorescence; polarized fluorescence; portable device.

Paper 170529RRR received Aug. 8, 2017; accepted for publication Dec. 21, 2017; published online Jan. 16, 2018.

## 1 Introduction

Globally, cervical cancer is the fourth most common cancer in women, with incidence rate of 7.9% and mortality rate of 7.5%.<sup>1</sup> Mortality due to cervical cancer can be minimized by detection at an early stage. Conventional methods for detection of cervical cancer are Pap smear (Papanicolaou test) and colposcopy followed by biopsy and the histopathological examination for final diagnosis and grading. Recent studies have suggested the use of the human papillomavirus test as one of the conventional tests for cervical cancer detection, which has comparatively high sensitivity and specificity. However, high risk positive patients still have to undergo yearly Pap tests to check any cell changes.<sup>1-4</sup> These conventional techniques are time consuming and limited in sensitivity or specificity,<sup>3,5-7</sup> which indicates that many samples are overcalled or missed. To overcome this limitation, a technique that is more accurate, fast, and minimally invasive is needed. Optical detection methods such as fluorescence spectroscopy, elastic scattering, and imaging have the potential for early diagnosis and are able to monitor cellular and chemical changes with disease progression.<sup>8-32</sup> Fluorescence spectroscopy is one of the relatively sensitive methods to probe subtle biochemical changes and this has been used for *in vitro* and *in vivo* studies over the past three

decades.<sup>8-18</sup> Since the fluorescence from tissue is significantly modified by absorption and scattering effects at both excitation and emission wavelengths, important diagnostic information of biochemical changes with disease progression are hidden. It is thus necessary to extract intrinsic fluorescence.<sup>23,33-39</sup> We have earlier developed an algorithm based on measured polarized fluorescence and polarized elastic scattering to extract intrinsic fluorescence, validated and tested it on tissue-mimicking phantoms and biological tissue samples with a commercial spectrofluorometer.<sup>34,35,39</sup> The intrinsic fluorescence is free from the distortion effects and hence provides more precise information about biochemical changes compared to the co-, cross-, and unpolarized spectrum.<sup>33-39</sup>

In this paper, we report *ex vivo* results of an in-house fabricated portable device, for detection of early stage cervical cancer by using polarized light at 405 nm excitation. The dominating fluorophore at this wavelength is flavin adenine dinucleotide (FAD)<sup>27,28,40,41</sup> with contributions from porphyrin.<sup>40,41</sup> With the progression of disease, FAD is known to change to its reduced form, which does not fluoresce.<sup>40-42</sup> It is also well known that deficiency of the enzyme ferrochelatase in tumors results in accumulation of porphyrin but not in the normal tissue.<sup>27,40,41</sup> Our results indicate that the contribution of intrinsic fluorescence of normal cervical tissue is higher than the

\*Address all correspondence to: Asima Pradhan, E-mail: [asima@iitk.ac.in](mailto:asima@iitk.ac.in)

abnormal signal. A principal component analysis (PCA) is applied on the spectra, and Mahalanobis distances (MD) and linear discrimination analysis (LDA) are used for classification of different precancers of cervix.

## 2 Materials and Methods

### 2.1 Instrumentation

A schematic diagram, cartoon, and photograph of the instrument fabricated in-house are shown in Figs. 1(a)–1(c). The device consists of two light sources, a laser diode (405 nm, Pegasus, Shanghai, Optical System Co. Ltd.) and a Xe-lamp (Newport Oriel Instruments) to measure polarized fluorescence and polarized elastic scattering spectra, respectively. Vertically polarized light is incident on a sample through beam splitters and lenses and by rotating the analyzer, co- and crosspolarized spectra are recorded. A high pass filter (450 nm cut off) is used to eliminate source effect. Signal is directed to a spectrometer (HR2000+, Ocean Optics, Inc., Dunedin, Florida) through an optical fiber and spectra recorded.

### 2.2 Sample Handling and Analysis Method

The study protocol was reviewed and approved by the institutional review board at the IIT Kanpur, India, and GSVM Medical College Kanpur, India. All samples were taken from hysterectomy cases and a written consent form was obtained from each patient by the doctors involved in this study. The protocol number for this work from the Institute Ethical Committee (IEC) of IIT Kanpur was IITK/IEC/2012-13/1/3. Studies using

the probe were performed on whole uterus samples directly after hysterectomy in the GSVM medical college.

Figure 1(d) shows the photograph of the cervix where the 12 o'clock position is selected as a reference point, while inner and outer circles show loci of the points in T-zone and outer-zone areas, respectively. Data are taken every 30 deg from the 12 o'clock position. T-zone area is an area of the cervix where endocervical cells (columnar cells) convert to ectocervical cells (squamous cells) and cervical cancer almost always originates from this area [Fig. 1(d)]. The whole uterus was first placed suitably (with the cervix area open to the probe) in a perspex box immediately after hysterectomy and measurements were taken from the cervix of the whole uterus. For the collection of data, a reference position was selected and tagged as 12 o'clock, and measurements taken at every 30 deg interval as shown in Fig. 1(d). Before recording the spectra, samples were rinsed with saline water to remove blood from the surface of the cervix. After experiments, these samples were sent to the pathology laboratory of GSVM medical college for histopathology. Polarized fluorescence and elastic scattering spectra for copolarized and crosspolarized states were recorded with incident polarized light. For fluorescence, the sample was illuminated with 405-nm wavelength and for elastic scattering, sample was illuminated with white light from a xenon arc lamp. Although intensities as well as integration times of these two sources were different, they were kept constant throughout the study for all samples and background corrections were performed for fluorescence and elastic scattering measurements separately. Measurements were taken from a total of 62 sites from T-zone and 94 sites from outer-zone areas of the cervix of 28 patients. The patients were from different age groups

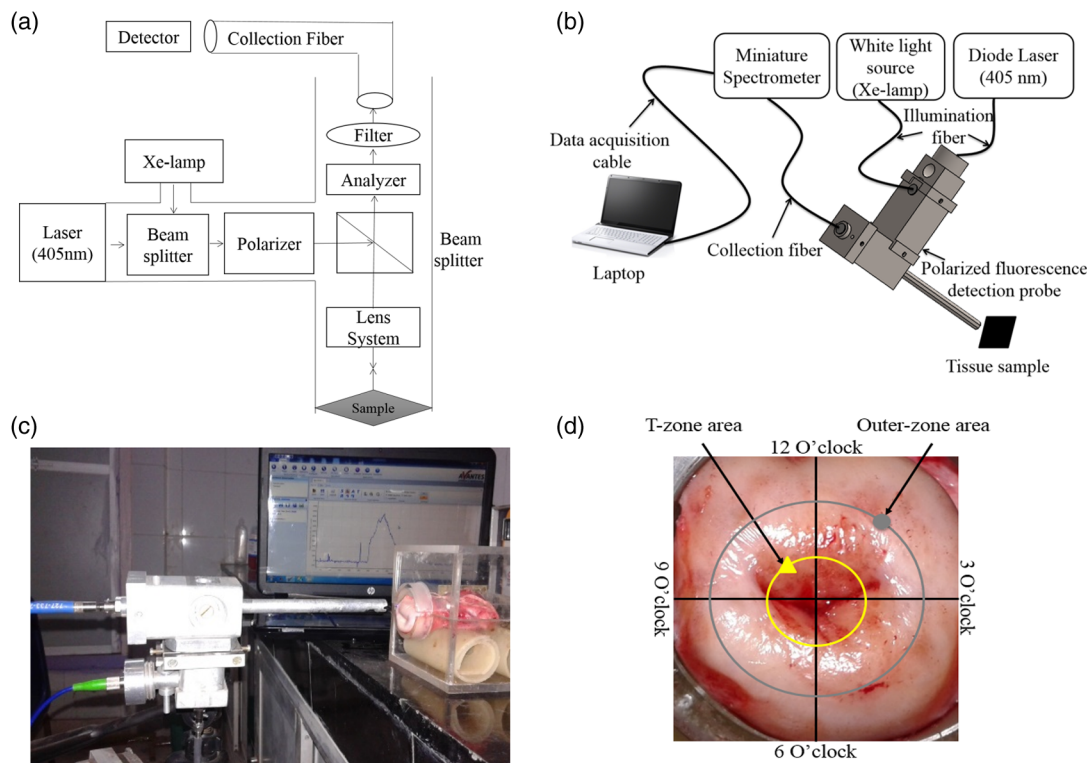


**Fig. 1** (a) Block diagram, (b) cartoon, and (c) photograph of system for polarized fluorescence measurements, showing light delivery to sample through optical fiber, other associated optical components and collection fiber. (d) Photograph of cervix showing the points in T-zone and outer-zone areas from where data are taken during the experiment.

**Table 1** Number of subjects and sites from different categories used in this study (age: 45 to 65 years).

	Prebiopsy diagnosis (colposcopy findings)	Postbiopsy diagnosis (histopathology findings)	Spectroscopic diagnosis
Number of subjects (sites)	28 (156)	28 (156)	28 (156)
Abnormal (sites)	16 (98)	15 (88)	15 (88)
Normal (sites)	12 (58)	13 (68)	13 (68)
CIN I (sites)	—	13 (72)	13 (72)
CIN II (sites)	—	2 (16)	2 (16)

(45 to 65 years) and economic backgrounds. Table 1 shows data sets of different categories of the cervix of the whole uterus based on prebiopsy, postbiopsy, and spectroscopy findings. Spectroscopy measurements were performed on two to five sites of each sample. In some cases where the cervix was wide open, measurements were done from eight sites. Comparison of spectral data and histopathology of each uterus sample was done and summarized as data for PCA.

The spectra are used in a multistep classification process to determine the tissue type of any unknown sample. This multistep classification process consists of the following steps: (1) extraction of intrinsic fluorescence, (2) use of principal components analysis to reduce the dimension of data, and (3) classification of tissue samples using MD and linear discriminant analysis algorithms. We extract the intrinsic fluorescence through<sup>34,39</sup>

$$IF = \frac{[I_{vv}(\lambda) - G(\lambda) * I_{vh}(\lambda)]_{fl}}{[I_{vv}(\lambda) - G(\lambda) * I_{vh}(\lambda)]_{scat}}, \quad (1)$$

where  $I_{vv}(\lambda)$  and  $I_{vh}(\lambda)$  are co- and crosspolarized signal and  $G(\lambda) [= I_{hh}(\lambda)/I_{hv}(\lambda)]$  is the ratio of the sensitivity of instruments to the vertically and horizontally polarized light, keeping the source light in horizontal polarized state. Here, the subscripts “fl” and “scat” represent fluorescence and elastic scattering, respectively. The polarized fluorescence and polarized elastic scattering spectra, which are free from diffuse elastic scattering effect, were generated by subtracting crosspolarized signal from copolarized signal. The copolarized signal goes through a small number of scattering events before the polarization is randomized. This component of the signal is the reduced component. On randomization, the components of both polarizations are equal and are the diffuse components of co- and crosspolarizations. The reduced component of the crosspolarized signal is negligible. A difference of co- and crosspolarized states thus retains only the reduced component of the copolarized signal, whereby scattering effects are almost eliminated. Normalizing polarized fluorescence spectrum  $[I_{vv}(\lambda) - G(\lambda) * I_{vh}(\lambda)]_{fl}$  with polarized elastic spectrum  $[I_{vv}(\lambda) - G(\lambda) * I_{vh}(\lambda)]_{scat}$  corresponding to the same wavelength range of fluorescence spectrum reduces the absorption effects. The validation of this technique has been previously reported on tissue mimicking phantoms and on *in vitro* measurements with cervical tissue samples.<sup>34,35,39</sup>

**Table 2** Training and validation data sets of all sites for MD calculation.

Tissue class	Training data	Validation data
Normal	34	34
CIN I	36	36
CIN II	8	8

The technique has also been validated using the fabricated device with tissue-mimicking liquid phantoms. Both spectral shape and intensity of original fluorescence spectra were recovered from a fluorophore in the turbid medium. The probe was subsequently tested on cervical biopsy tissue samples with promising results using the same classification described below.

After extraction of intrinsic fluorescence, PCA was applied for dimension reduction, after which the scores of the principal components (eigenvectors) of the spectra, which contain maximum variance of the complete data were determined.<sup>13,39,43</sup> In this case, the first seven principal components PC1, PC2, PC3, PC4, PC5, PC6, and PC7 corresponding to the first seven eigenvalues of the correlation matrix of whole data were calculated, which captured almost more than 99% variance of the original data. Subsequently, MDs and LDA were used to classify the tissue grades. The scores of selected principal components (PCs) of each sample group were divided into training and validation data sets and the MDs from the validation data sets ( $v$ ) to the centroid of training data ( $t_m$ ) set points of each tissue class were calculated with the help of following Mahalanobis equation:<sup>39,43–45</sup>

$$r = \sqrt{(v - t_m)' * c_t^{-1} * (v - t_m)}, \quad (2)$$

where  $c_t$  is the covariance matrix for the training data set of that tissue sample class. The training and validation grouping was done on the basis of the sites from different categories of the sample as shown in Table 1. An unknown sample was classified according to the minimum distance  $r$  from the centroid of a particular class. To avoid the biasedness and validate the results of this multivariate approach in classifying the unknown sample, the data sets of the two tissue types were each divided randomly into two groups, with one half of the sample from each class taken as the training set and the other half taken as the validation set. Selection of training and validation data sets for this study is shown in Table 2.

MDs were calculated using the training data set for each class and each validation sample was classified by selecting the neighborhood for which the distance to the validation sample was minimum. This was repeated by taking randomly selected samples in training and validation data sets and no significant differences in classification could be seen. Further, the same scores of selected PCs of each sample group were taken and LDA was used to classify all three classes together.

### 3 Results and Discussion

Figures 2(a)–2(b) show the copolarized, crosspolarized, polarized fluorescence, polarized elastic scattering, and intrinsic fluorescence spectra from a typical cervical intraepithelial neoplasia (CIN) I sample with 405-nm excitation wavelength. A broad fluorescence profile with peak at 505 nm is obtained, which is ascribed to FAD.<sup>27,28,40,41</sup> Although the major

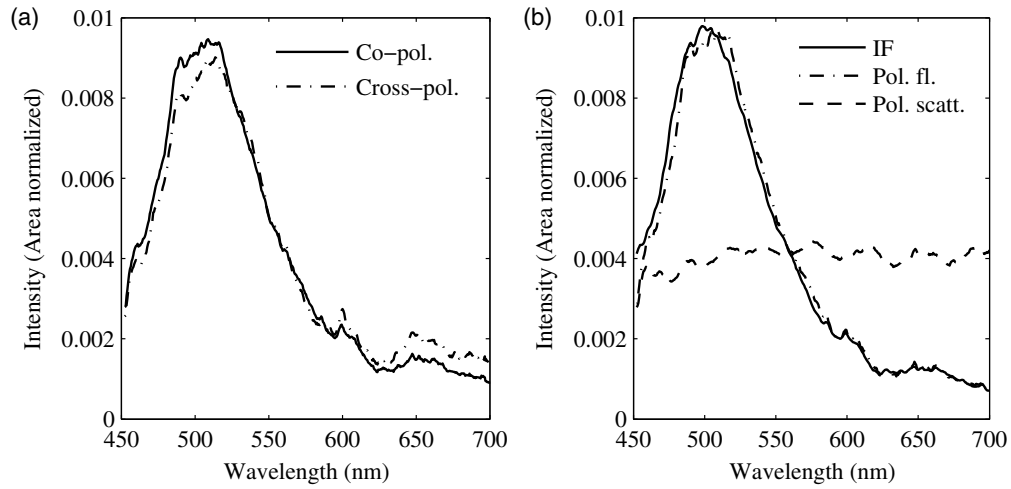


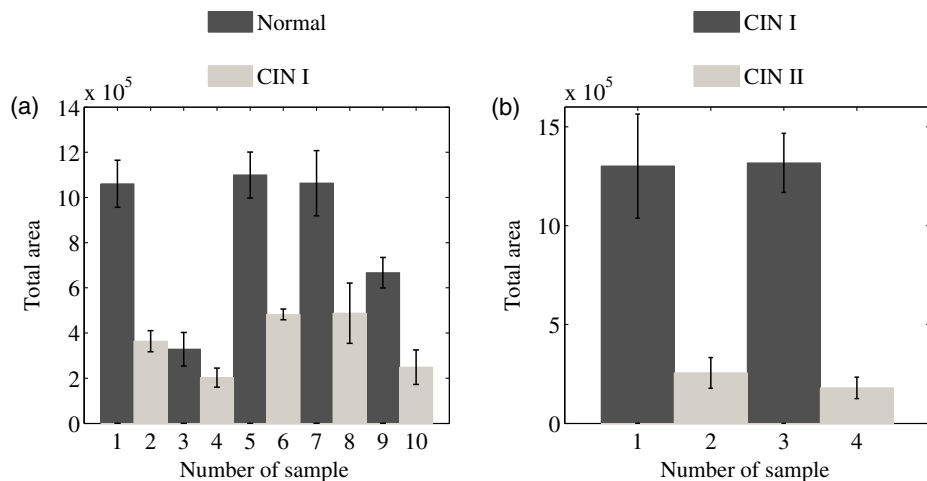
**Fig. 2** Typical plots of (a) co- and crosspolarized fluorescence, (b) polarized fluorescence, polarized elastic scattering, and intrinsic fluorescence spectra.

contributing fluorophore at 405 nm excitation wavelength is FAD, NADH and porphyrin also show their signatures. The characteristic absorption dips of hemoglobin (Hb)/oxygenated Hb and porphyrin absorption, at 476 nm, 527 and 556 nm can be seen in both polarized fluorescence and polarized elastic scattering spectra in Fig. 2(b). As expected, normalizing polarized fluorescence with polarized scattering eliminates the absorption dips and recovery of spectral line shape is clearly visible in the intrinsic fluorescence spectra of Fig. 2(b). The change in the area under the curve of fluorescence spectra averaged over all the sites of the T-zone of each subject with their corresponding counterparts in the outer zone are displayed in Figs. 3(a) and 3(b). The area under the curve is seen to decrease from normal to increasing grades of precancer, which confirms the decrease in contribution of the major fluorophore (FAD) due to its conversion to the reduced nonfluorescent form with disease progression.<sup>40-42</sup>

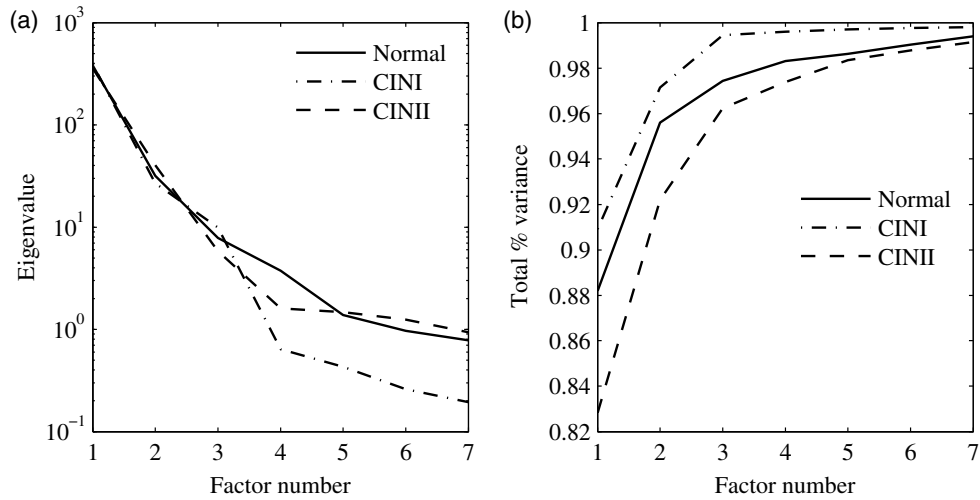
Figures 4(a) and 4(b) show the weightage distribution of eigenvalues and total percentage variance of the eigenvalues, respectively. This shows that even though the eigenvalue contributions with seven PCs are drastically decreased, the variance

is found to be 99%. Hence, seven PCs were used in the analysis. Figures 5(a) and 5(b) show the reconstruction of the original data with the first six and first seven PCs, respectively. It can be seen that the reconstruction of the spectra with the first six PCs is not as good as that with the first seven PCs. Figure 6 shows the scatter plot of MD of each sample from the training centroids of an individual class for discrimination of tissue grades. In Fig. 6(a), the samples that lie farthest from x-axis are characterized as normal and samples farthest from y-axis are CIN I, which are separated by a discrimination line at 45 deg angle with respect to x and y axes. Figures 6(b) and 6(c) similarly show the discrimination between normal and CIN II and CIN I and CIN II samples, respectively.

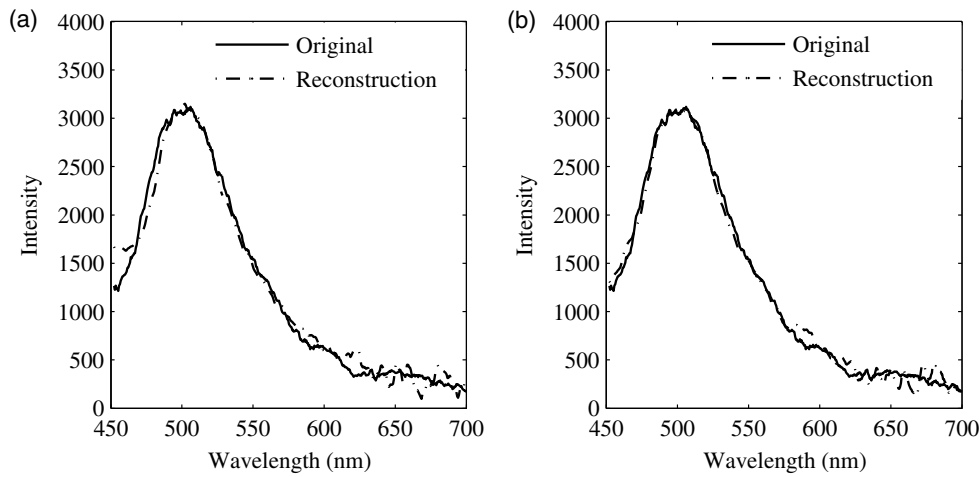
Sensitivity and specificity are found from results of scatter plots and statistical findings are shown in Table 3. Excellent discrimination of CIN I and CIN II from corresponding normal samples is obtained and CIN I can also be distinguished from CIN II with a very high sensitivity. Figure 7 shows the scatter plot of first and second linear discriminants (LD1 and LD2) of normal, CIN I, and CIN II. The statistical findings of LDA are given in Table 3. It is pertinent to note that results different



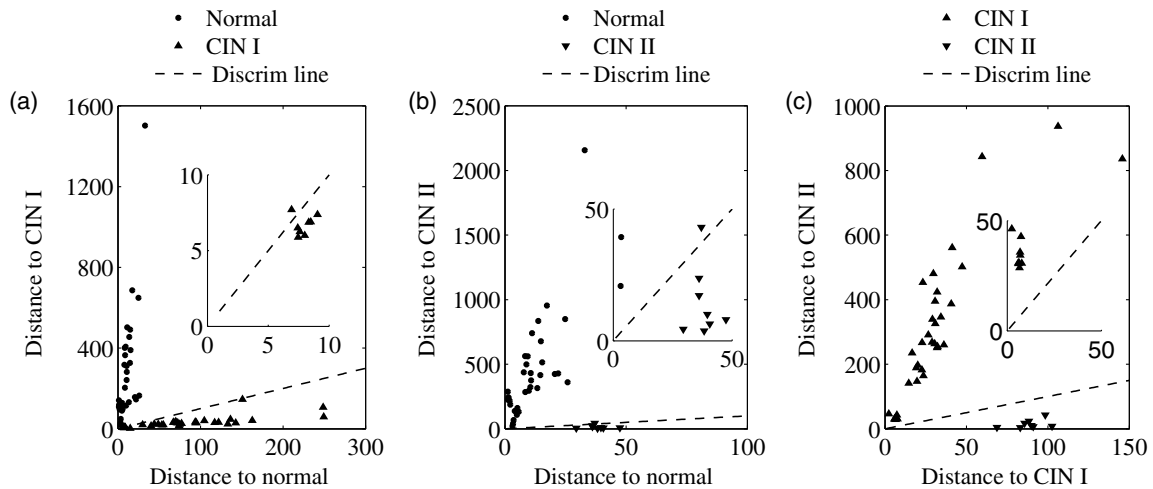
**Fig. 3** Comparison of intensity variation of intrinsic fluorescence from cervix of whole uterus samples (average of measured sites of each sample with standard deviation) with disease progression (a) normal versus CIN I and (b) CIN I versus CIN II.



**Fig. 4** Plots of (a) selected eigenvalues and (b) the total percent variance of the selected eigenvalues of PCA for normal, CIN I, and CIN II samples.



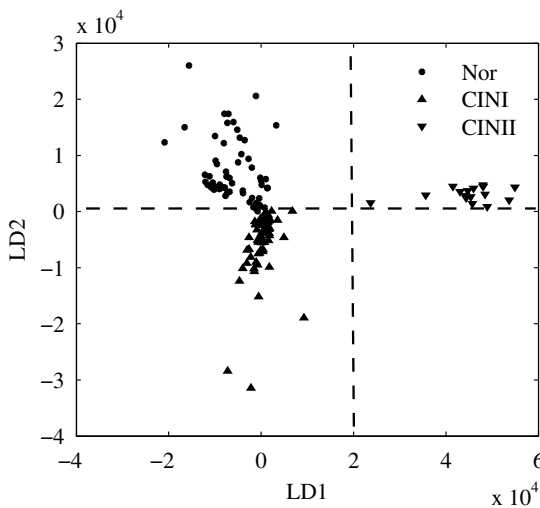
**Fig. 5** Typical plots of original and reconstructed spectra of normal data with (a) first six principal components and (b) first seven principal components.



**Fig. 6** Scatter plots of MD using intrinsic fluorescence from each site of the cervix of different uterus samples to the training centroids of the individual class for discrimination; (a) normal versus CINI, (b) normal versus CINII, and (c) CINI versus CINII (insets show the magnified view around the origin).

**Table 3** Statistical results of classification of different tissue classes of hysterectomy samples (with 95% confidence level).

Tissue classes	Sensitivity	Specificity
MD		
Normal versus CIN I	91%	100%
Normal versus CIN II	87%	100%
CIN I versus CIN II	100%	100%
Linear discrimination analysis		
Normal versus CIN I	97%	98.5%
Normal versus CIN II	100%	100%
CIN I versus CIN II	100%	100%

**Fig. 7** Scatter plot of LD1 versus LD2 for normal, CIN I, and CIN II samples.

from these *in vivo* studies may require appropriate changes in the classification algorithm. These results indicate that our in-house fabricated portable device based on polarized fluorescence and elastic scattering measurements has the potential to diagnose cervical precancer *in vivo* and can be a part of regular screening techniques for cervical precancer detection.

### Disclosures

The authors have no relevant financial interests in this article and no potential conflicts of interest to disclose.

### Acknowledgments

Asima Pradhan wishes to acknowledge the Department of Science & Technology (DST), Govt. of India (grant number IDP/MED/2013/08) and the Society for Research and Initiatives for Sustainable Technologies and Institutions (SRISTI), Ahmedabad, Gujarat, India (grant number BIRAC/PHY/2016353) for funding the research. Bharat Lal Meena acknowledges Council of Scientific and Industrial Research (CSIR), India for providing fellowship and Society for

Research and Initiatives for Sustainable Technologies and Institutions (SRISTI), Ahmedabad, Gujarat, India, for funding the research (grant number BIRAC/PHY/2016353).

### References

1. C. P. Wild and B. W. Stewart, *World Cancer Report 2014*, World Health Organization (2014).
2. C. J. Meijer et al., "Guidelines for human papillomavirus DNA test requirements for primary cervical cancer screening in women 30 years and older," *Int. J. Cancer* **124**(3), 516–520 (2009).
3. A. Longatto-Filho et al., "Performance characteristics of Pap test, via, VILI, HR-HPV testing, cervicography, and colposcopy in diagnosis of significant cervical pathology," *Virchows Arch.* **460**(6), 577–585 (2012).
4. A. Hesselink et al., "Clinical validation of Anyplex™ II HPV HR detection according to the guidelines for HPV test requirements for cervical cancer screening," *J. Clin. Virol.* **76**, 36–39 (2016).
5. M. Karimi-Zarchi et al., "A comparison of 3 ways of conventional Pap smear, liquid-based cytology and colposcopy vs. cervical biopsy for early diagnosis of premalignant lesions or cervical cancer in women with abnormal conventional Pap test," *Int. J. Biomed. Sci.* **9**(4), 205 (2013).
6. D. G. Ferris et al., "Colposcopy quality control by remote review of digitized colposcopic images," *Am. J. Obstet. Gynecol.* **191**(6), 1934–1941 (2004).
7. L. S. Massad et al., "The accuracy of colposcopic grading for detection of high grade cervical intraepithelial neoplasia," *J. Lower Genital Tract Dis.* **13**(3), 137–144 (2009).
8. R. Alfano et al., "Fluorescence spectra from cancerous and normal human breast and lung tissues," *IEEE J. Quantum Electron.* **23**(10), 1806–1811 (1987).
9. G. Tang et al., "Pulsed and CW laser fluorescence spectra from cancerous, normal, and chemically treated normal human breast and lung tissues," *Appl. Opt.* **28**(12), 2337–2342 (1989).
10. M. Keijzer et al., "Fluorescence spectroscopy of turbid media: autofluorescence of the human aorta," *Appl. Opt.* **28**(20), 4286–4292 (1989).
11. R. Richards-Kortum et al., "In vivo fluorescence spectroscopy: potential for non-invasive, automated diagnosis of cervical intraepithelial neoplasia and use as a surrogate endpoint biomarker," *J. Cell. Biochem.* **19**(Suppl.), 111–119 (1994).
12. N. Ramanujam et al., "In vivo diagnosis of cervical intraepithelial neoplasia using 337-nm-excited laser-induced fluorescence," *Proc. Natl. Acad. Sci. U. S. A.* **91**(21), 10193–10197 (1994).
13. N. Ramanujam et al., "Spectroscopic diagnosis of cervical intraepithelial neoplasia (CIN) in vivo using laser-induced fluorescence spectra at multiple excitation wavelengths," *Lasers Surg. Med.* **19**(1), 63–74 (1996).
14. R. Drezek et al., "Understanding the contributions of NADH and collagen to cervical tissue fluorescence spectra: modeling, measurements, and implications," *J. Biomed. Opt.* **6**(4), 385–396 (2001).
15. A. H. Gharekhan et al., "Characteristic spectral features of the polarized fluorescence of human breast cancer in the wavelet domain," *Appl. Spectrosc.* **66**(7), 820–827 (2012).
16. K. Sokolov, M. Follen, and R. Richards-Kortum, "Optical spectroscopy for detection of neoplasia," *Curr. Opin. Chem. Biol.* **6**(5), 651–658 (2002).
17. Y. N. Mirabal et al., "Reflectance spectroscopy for in vivo detection of cervical precancer," *J. Biomed. Opt.* **7**(4), 587–594 (2002).
18. K. T. Schomacker et al., "Novel optical detection system for in vivo identification and localization of cervical intraepithelial neoplasia," *J. Biomed. Opt.* **11**(3), 034009 (2006).
19. K. Vishwanath et al., "Portable, fiber-based, diffuse reflection spectroscopy (DRS) systems for estimating tissue optical properties," *Appl. Spectrosc.* **65**(2), 206–215 (2011).
20. R. J. Mallia et al., "Clinical grading of oral mucosa by curve-fitting of corrected autofluorescence using diffuse reflectance spectra," *Head Neck* **32**(6), 763–779 (2010).
21. H.-W. Wang, Y.-H. Wei, and H.-W. Guo, "Reduced nicotinamide adenine dinucleotide (NADH) fluorescence for the detection of cell death," *Anticancer Agents Med. Chem.* **9**(9), 1012–1017 (2009).

22. S. M. Chidananda et al., "Optical diagnosis of cervical cancer by fluorescence spectroscopy technique," *Int. J. Cancer* **119**(1), 139–145 (2006).
23. R. S. Bradley and M. S. Thorniley, "A review of attenuation correction techniques for tissue fluorescence," *J. R. Soc. Interface* **3**(6), 1–13 (2006).
24. J. A. Freeberg et al., "The clinical effectiveness of fluorescence and reflectance spectroscopy for the in vivo diagnosis of cervical neoplasia: an analysis by phase of trial design," *Gynecol. Oncol.* **107**(1), S270–S280 (2007).
25. A. B. Rodero et al., "Fluorescence spectroscopy for diagnostic differentiation in uteris cervix biopsies with cervical/vaginal atypical cytology," *J. Fluoresc.* **18**(5), 979–985 (2008).
26. M. Olivo, C. J. H. Ho, and C. Y. Fu, "Advances in fluorescence diagnosis to track footprints of cancer progression in vivo," *Laser Photonics Rev.* **7**(5), 646–662 (2013).
27. J. Lakowicz, *Principles of Fluorescence Spectroscopy*, Springer, New York (2007).
28. R. Alfano and Y. Yang, "Stokes shift emission spectroscopy of human tissue and key biomolecules," *IEEE J. Sel. Top. Quantum Electron.* **9**(2), 148–153 (2003).
29. N. Ramanujam, "Fluorescence spectroscopy of neoplastic and non-neoplastic tissues," *Neoplasia* **2**(1–2), 89–117 (2000).
30. S. H. Tabrizi et al., "The use of optical spectroscopy for in vivo detection of cervical pre-cancer," *Lasers Med. Sci.* **29**(2), 831–845 (2014).
31. B. Yu et al., "Emerging optical techniques for detection of oral, cervical and anal cancer in low-resource settings," *Austin J. Biomed. Eng.* **1**(2), 1007 (2014).
32. V. G. Prabitha et al., "Detection of cervical lesions by multivariate analysis of diffuse reflectance spectra: a clinical study," *Lasers Med. Sci.* **31**(1), 67–75 (2016).
33. J. Wu, M. S. Feld, and R. P. Rava, "Analytical model for extracting intrinsic fluorescence in turbid media," *Appl. Opt.* **32**(19), 3585–3595 (1993).
34. N. C. Biswal et al., "Recovery of turbidity free fluorescence from measured fluorescence: an experimental approach," *Opt. Express* **11**(24), 3320–3331 (2003).
35. D. Rath et al., "A comparative study of intrinsic versus bulk polarized fluorescence in cervical tissues," *Proc. SPIE* **6853**, 685319 (2008).
36. S. Gupta, V. S. Raja, and A. Pradhan, "Simultaneous extraction of optical transport parameters and intrinsic fluorescence of tissue mimicking model media using a spatially resolved fluorescence technique," *Appl. Opt.* **45**(28), 7529–7537 (2006).
37. G. M. Palmer and N. Ramanujam, "Monte-Carlo-based model for the extraction of intrinsic fluorescence from turbid media," *J. Biomed. Opt.* **13**(2), 024017 (2008).
38. M. G. Müller et al., "Intrinsic fluorescence spectroscopy in turbid media: disentangling effects of scattering and absorption," *Appl. Opt.* **40**(25), 4633–4646 (2001).
39. S. Devi, P. K. Panigrahi, and A. Pradhan, "Detecting cervical cancer progression through extracted intrinsic fluorescence and principal component analysis," *J. Biomed. Opt.* **19**(12), 127003 (2014).
40. R. Richards-Kortum and E. Sevick-Muraca, "Quantitative optical spectroscopy for tissue diagnosis," *Annu. Rev. Phys. Chem.* **47**(1), 555–606 (1996).
41. S. Madhuri et al., "Native fluorescence spectroscopy of blood plasma in the characterization of oral malignancy," *Photochem. Photobiol.* **78**(2), 197–204 (2003).
42. R. Alfano et al., "Laser induced fluorescence spectroscopy from native cancerous and normal tissue," *IEEE J. Quantum Electron.* **20**(12), 1507–1511 (1984).
43. S. K. Chang et al., "Combined reflectance and fluorescence spectroscopy for in vivo detection of cervical pre-cancer," *J. Biomed. Opt.* **10**(2), 024031 (2005).
44. R. De Maesschalck, D. Jouan-Rimbaud, and D. L. Massart, "The Mahalanobis distance," *Chemom. Intell. Lab. Syst.* **50**(1), 1–18 (2000).
45. H. L. Mark and D. Tunnell, "Qualitative near-infrared reflectance analysis using Mahalanobis distances," *Anal. Chem.* **57**(7), 1449–1456 (1985).

**Bharat Lal Meena** is a research scholar at the Indian Institute of Technology (IIT), Kanpur and an assistant professor at the University of Rajasthan, Jaipur. He received his MS degree in physics from the University of Delhi in 2010. His research interests have been in the area of biophotonics. The recent focus lies in the development of a portable device for detection of cervical cancer at an early stage using polarized light.

**Asima Pradhan** is a professor in the Department of Physics at IIT, Kanpur, India, and is also associated with the Center for Lasers and Photonics. She received her PhD from the City University of New York in 1991. Her areas of interest include laser spectroscopy and biophotonics. Her expertise is in fluorescence spectroscopy, light scattering spectroscopy, time-resolved fluorescence, polarization-based fluorescence, and Mueller matrix imaging of biosamples.

Biographies for the other authors are not available.